







<https://doi.org/10.1038/s42003-023-04792-4>

OPEN

Structure of anhydrotetracycline-bound Tet(X6) reveals the mechanism for inhibition of type 1 tetracycline destructases

Hirdesh Kumar¹, Emily E. Williford², Kevin S. Blake ³, Brett Virgin-Downey², Gautam Dantas ^{3,4,5,6,7}✉, Timothy A. Wencewicz ²✉ & Niraj H. Tolia ¹✉

Inactivation of tetracycline antibiotics by tetracycline destructases (TDases) remains a clinical and agricultural threat. TDases can be classified as type 1 Tet(X)-like TDases and type 2 soil-derived TDases. Type 1 TDases are widely identified in clinical pathogens. A combination therapy of tetracycline and a TDase inhibitor is much needed to rescue the clinical efficacy of tetracyclines. Anhydrotetracycline is a pan-TDase inhibitor that inhibits both type 1 and type 2 TDases. Here, we present structural, biochemical, and phenotypic evidence that anhydrotetracycline binds in a substrate-like orientation and competitively inhibits the type 1 TDase Tet(X6) to rescue tetracycline antibiotic activity as a sacrificial substrate. Anhydrotetracycline interacting residues of Tet(X6) are conserved within type 1 TDases, indicating a conserved binding mode and mechanism of inhibition. This mode of binding and inhibition is distinct from anhydrotetracycline's inhibition of type 2 TDases. This study forms the framework for development of next-generation therapies to counteract enzymatic tetracycline resistance.

¹Host-pathogen interaction and structural vaccinology section (HPISV), National Institute of Allergy and Infectious Diseases (NIAID), National Institutes of Health (NIH), Bethesda, MD, USA. ²Department of Chemistry, Washington University in St. Louis, One Brookings Drive, St. Louis, MO 63130, USA. ³The Edison Family Center for Genome Sciences and Systems Biology, Washington University School of Medicine, St. Louis, MO, USA. ⁴Department of Pathology and Immunology, Division of Laboratory and Genomic Medicine, Washington University School of Medicine, St. Louis, MO, USA. ⁵Department of Molecular Microbiology, Washington University School of Medicine, St. Louis, MO, USA. ⁶Department of Biomedical Engineering, Washington University in St. Louis, St. Louis, MO, USA. ⁷Department of Pediatrics, Washington University School of Medicine, St. Louis, MO, USA. ✉email: dantas@wustl.edu; wencewicz@wustl.edu; niraj.tolia@nih.gov

Tetracyclines are a class of broad-spectrum antibiotics widely used in clinical and agricultural settings, and considered one of the big four antibiotics for human use¹. Intensive use for more than eight decades has given rise to high abundance and diversity of tetracycline resistance genes in clinical pathogens. Historically, the two main mechanisms of tetracycline resistance have been ribosomal protection and drug efflux². To maintain the efficacy of this drug class against antibiotic resistance by these mechanisms, third-generation tetracyclines have been recently developed by chemical modification of the tetracycline moiety^{3–5}. Of these third-generation drug molecules, tigecycline is a last resort antibiotic used to treat infections with multidrug resistant (MDR) gram-negative bacteria and extensively drug-resistant (XDR) *Enterobacteriaceae* and *Acinetobacter* species^{6,7}.

Although tigecycline and other last-generation tetracyclines circumvent resistance by ribosomal protection or efflux pumps, these molecules are inactivated by a group of enzymes called tetracycline destructases (TDases)^{8,9}. In recent years, we and others have identified and characterized a plethora of TDases found in commensal, environmental, and pathogenic bacteria^{10–15}. TDases are class A flavin-dependent mono-oxygenases that covalently modify and inactivate the core tetracycline moiety. Enzymatic inactivation of tetracyclines is unique in comparison to canonical tetracycline-resistance mechanisms because inactivation renders the tetracycline molecule incapable of further activity. TDases are broadly classified into two types based on sequence-structure-function characteristics: Tet(X)-like TDases and soil-derived TDases. Tet(X)-like TDases, which include the prototypical Tet(X) enzyme, have been identified in human gut metagenomes and pathogens, and can inactivate tetracyclines of all generations, including tigecycline and recently FDA-approved drugs sarecycline, eravacycline and omadacycline^{10,12}. In contrast, soil-derived TDases have been primarily identified in soil metagenomes, and can inactivate first- and second- generation tetracyclines, but show limited activity against last-generation tetracyclines¹⁶. However, this soil-derived group of TDases can also be identified from other ecosystems. Tet(X)-like TDases and soil-derived TDases share only ~20% amino acid similarity and they have broadly similar structures^{12,14,17,18}. Therefore, we propose naming these two classes of TDases as type 1 TDases for Tet(X)-like TDases; and type 2 TDases for those originally identified in soil metagenomes. A potent TDase inhibitor is needed for use in combination therapy to rescue the efficacy of the tetracycline group of antibiotics against pathogens expressing TDases.

Anhydrotetracycline (aTC) is the first broad spectrum TDase inhibitor that blocks type 1 and type 2 TDases in vitro and in bacterial phenotypic assays¹². We previously reported the crystal structure of anhydrotetracycline bound to the type 2 TDase Tet(50), showing it is a competitive inhibitor that binds in a distinct mode in the substrate binding cavity¹²; these structural insights enabled development of anhydrotetracycline derivatives as additional type 2 TDase inhibitors¹⁹. However, the binding and inhibition mode of anhydrotetracycline to type 1 TDases are unknown.

Here, we investigate Tet(X6), a type 1 TDase first discovered in a *Proteus* genomospecies²⁰, by determining anhydrotetracycline-free and anhydrotetracycline-complexed X-ray crystal structures. Tet(X6) inactivates all classes of tetracyclines demonstrated by in vitro enzyme assays and phenotypic studies in *E. coli*. The whole cell growth inhibitory activity of tetracycline against *E. coli* expressing Tet(X6) is rescuable with anhydrotetracycline. The structures revealed that anhydrotetracycline binds in a substrate-like orientation in Tet(X6) and serves as a competitive inhibitor. In contrast, type 2 TDases are unable to metabolize

anhydrotetracycline, and anhydrotetracycline binds to type 2 TDases in a distinct orientation as a mechanistic and competitive inhibitor¹². Michaelis-Menten steady-state kinetic studies confirmed that anhydrotetracycline is a substrate for Tet(X6). Direct detection of the anhydrotetracycline Tet(X6) oxidation product by LC-MS further supports a model for competitive inhibition as a sacrificial substrate. The current study explains the differences in structural and functional characteristics of anhydrotetracycline between the two classes of TDases.

Results

Tet(X6) contains a conserved architecture of type 1 tetracycline destructases. We determined the X-ray structure of Tet(X6) at 2.2 Å resolution with R_{free}/R_{work} of 0.22/0.19 (Table 1). This FAD complexed, anhydrotetracycline-free enzyme structure consists of a conserved architecture for type 1 TDases: a characteristic Rossman fold containing an FAD-binding domain, a substrate binding domain, and a C-terminal bridge helix that connects the two domains (Fig. 1). The 393 amino acid long polypeptide chain alternates four times between the substrate-binding domain and FAD-binding domain. The Tet(X6) holo-enzyme resembles previously reported type 1 TDases with high structural similarity of <0.5 Å r.m.s.d. on C^α atoms, and high sequence identity of >85% (Supplementary Fig. 1)^{14,17,18}.

Tet(X6) contains a single C-terminal bridge helix similar to other type 1 TDase structures (Tet(X2) – PDB 2Y6R, Tet(X4) – PDB 7EPV, and Tet(X7) – PDB 6WG9) (Supplementary Fig. 1) and this constitutes a major distinction from type 2 TDases that contain a 2nd α -helix at the C-terminus¹² (Fig. 1 and Supplementary Fig. 2). The FAD cofactor is bound in an “IN” orientation in Tet(X6). Thus far, the FAD conformation in structures of type 1 TDases have only been captured in this “IN”

Table 1 Data Reduction Statistics for the Tet(X6) and Tet(X6) in complex with anhydrotetracycline structures.

	Tet(X6) (8ER1)	Tet(X6) + Anhydrotetracycline (8ERO)
Data collection		
Space group	P 1 21 1	P 1 21 1
Cell dimensions		
<i>a</i> , <i>b</i> , <i>c</i> (Å)	43.77, 52.49, 95.17	87.09, 52.21, 94.87
α , β , γ (°)	90, 95.88, 90	90, 95.44, 90
Resolution (Å)	19.9–1.9 (1.94–1.9)	19.84–2.2 (2.28–2.2)
<i>R</i> _{merge}	0.031 (0.234)	0.095 (0.592)
<i>I</i> / σ <i>I</i>	18.1 (2.8)	9.8 (5.1)
Completeness (%)	98.8 (98.0)	98.8 (98.0)
Redundancy	3.5 (3.3)	3.5 (3.4)
Refinement		
Resolution (Å)	19.9–1.9 (1.94–1.9)	19.84–2.2 (2.28–2.2)
No. reflections	33,536 (3273)	42,923 (4215)
<i>R</i> _{work} / <i>R</i> _{free}	0.20/0.23	0.19/0.23
No. atoms		
Protein	2952	5877
Ligands	84	268
Water	152	263
<i>B</i> -factors		
Protein	41.1	33.1
Ligands	33.6	38.7
Water	41.8	32.9
R.m.s. deviations		
Bond lengths (Å)	0.011	0.003
Bond angles (°)	1.09	0.57

Each structure was solved from a single crystal. Values in parentheses are for highest-resolution shell.

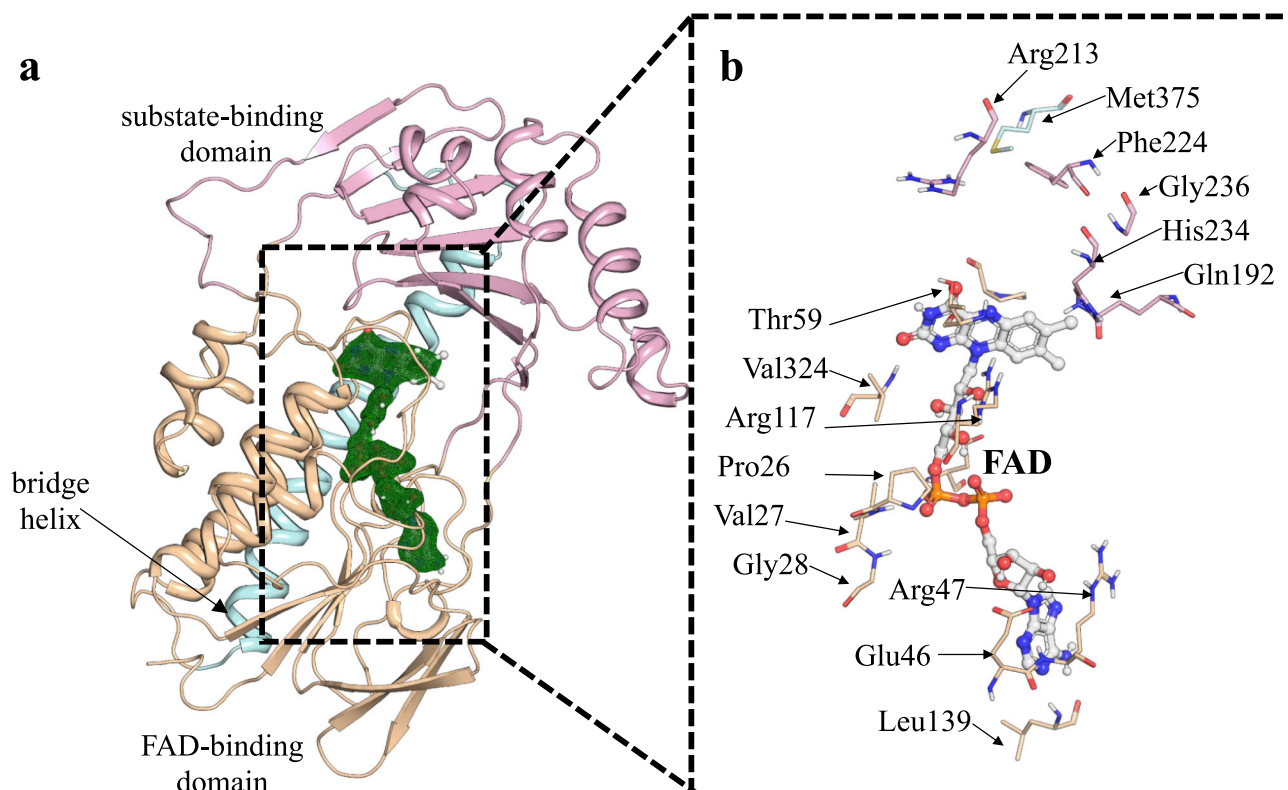


Fig. 1 Tet(X6) has a conserved architecture of type 1 TDases. **a** Structure of anhydrotetracycline free Tet(X6) determined here (8ER1). The substrate-binding domain is colored pink. The FAD-binding domain is colored orange. The C-terminal bridge helix is colored blue. Omit map for the bound FAD omitted from the Tet(X6) anhydrotetracycline free structure determined here (8ER1) is shown in green and density is contoured at 2.5σ . The FAD is bound in an “IN” orientation consistent with previously solved type 1 TDase structures. **b** Key residues in the Tet(X6) anhydrotetracycline free structure determined here (8ER1) that interact with FAD are shown. Residues in the substrate binding pocket are also highlighted. Color scheme: orange - residues from the FAD binding domain; pink - residues from the substrate binding domain; and blue - residues from the C-terminal bridge helix.

orientation, while structures of type 2 TDases have been solved for both “IN” and “OUT” orientations. It is assumed, but not yet experimentally validated, that the FAD cofactor present in the type 1 TDases share this two-state binding mode. The FAD-binding pocket and the substrate-binding pocket are conserved among all four of the solved type 1 TDase structures (Fig. 1 and Supplementary Fig. 1). The conserved FAD-interacting residues include Pro26, Val27, Gly28, Glu46, Arg47, Thr59, Arg117, Leu139, and Val324. The conserved substrate-binding residues are Gln192, Arg213, Phe224, His234 and Gly236. Met375 of the C-terminal bridge helix also interacts with the bound tetracycline substrate and is conserved among the type 1 TDases (Fig. 1 and Supplementary Figs. 1, 3). The asymmetric units and packing of crystal lattices of Tet(X6) X-ray crystal structures are shown in Supplementary Fig. 4. Despite structural similarities, type 1 TDases can show significant differences in enzyme kinetics with up to ~10-fold difference in apparent catalytic efficiency¹⁴. Mutations outside the TDase active site generated via directed evolution and natural selection have been shown to enhance enzyme efficiency and resistance levels in whole cell assays^{17,21}. It is likely that surface-exposed residues affect both conformational dynamics and active site environments of different TDases, leading to differences in protein stability and enzyme efficiency that influence resistance phenotypes. Additional putative binding sites have been observed at the entrance of the active site in the Tet(X)-minocycline complex crystal structure (PDB ID: 4A99) that could plausibly guide the substrate into the active site²².

Tet(X6) confers pan-tetracycline-resistance. We validated the activity of Tet(X6) in the *E. coli* DH5aZ1 + pZE24 system using

microbroth dilution antibiotic susceptibility tests²³ (Fig. 2a, b). For positive and negative controls, we also characterized the resistance profiles of *E. coli* strains producing Tet(X7) or containing the empty pZE24 vector (*i.e.*, with no tetracycline resistance gene). In accordance with the initial report on this enzyme²⁰, heterologous expression of Tet(X6) in *E. coli* conferred high minimal inhibitory concentrations (MICs) against tetracycline antibiotics from all three generations (Fig. 2b). The highest MICs were against first-generation drug molecules tetracycline and chlortetracycline (256 and 128 $\mu\text{g}/\text{mL}$, respectively). Consistent with other type 1 TDases, Tet(X6) also conferred resistance to doxycycline, a second-generation tetracycline, as well as third-generation tetracyclines tigecycline, omadacycline, and eravacycline^{5,24}. Notably, the Tet(X6) strain’s MICs are 2- to 8-fold higher than the Tet(X7) strain, which had been previously considered one of the most active TDases^{14,19} (Fig. 2b).

To study substrate binding and catalytic efficiency of Tet(X6) under steady state conditions, we continuously monitored the change in absorbance at 400 nm (unique λ_{max} for tetracyclines) to observe direct enzymatic inactivation of tetracycline substrates: tetracycline, tigecycline, omadacycline, and eravacycline by Tet(X6) (Fig. 2c, d). The velocity versus substrate concentration curves for tetracycline and tigecycline were hyperbolic with good fit to the standard Michaelis-Menten equation. The curves for eravacycline and omadacycline appeared sigmoidal in nature, indicating the potential for allostery or multiple binding orientations for the substrate, the latter of which has been observed for the TDase family^{12,18}. Curve fitting to Michaelis-Menten and allosteric sigmoidal models in GraphPad prism both produced acceptable fits ($R^2 > 0.95$) (Supplementary Fig. 5; Supplementary Data 1).

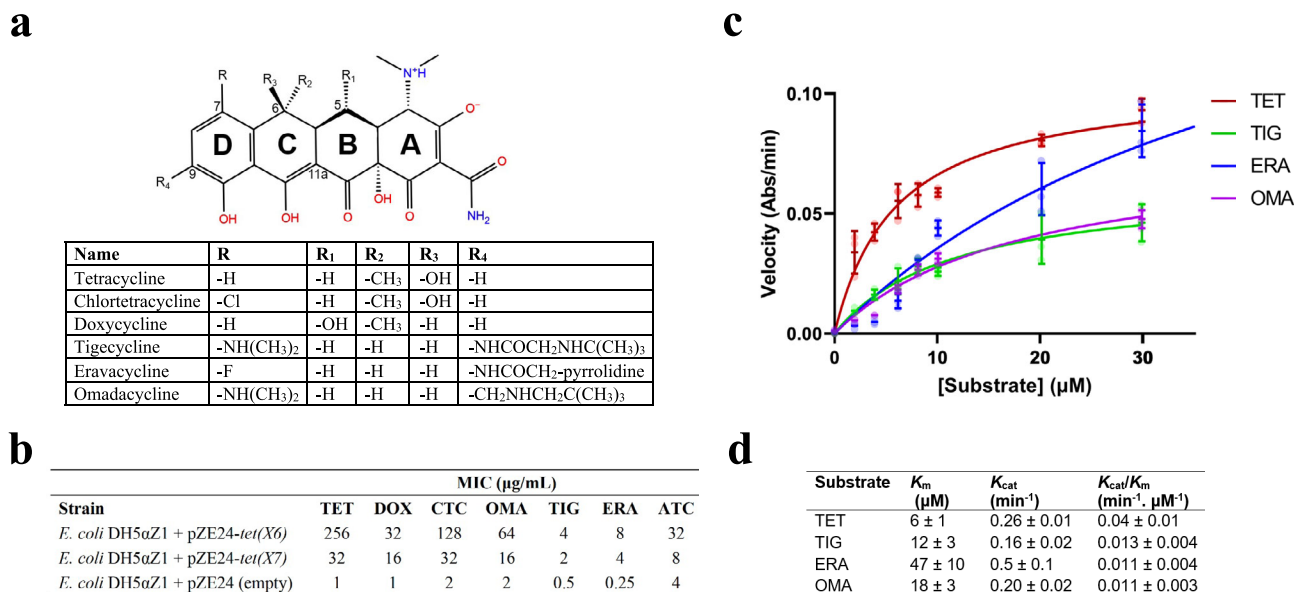


Fig. 2 Tet(X6) confers pan tetracycline resistance. **a** Chemical structures of different tetracyclines. **b** Tet(X6) confers high minimum inhibitory concentrations (MIC). Abbreviations: tetracycline (TET); doxycycline (DOX); chlortetracycline (CTC); omadacycline (OMA); tigecycline (TIG); eravacycline (ERA); anhydrotetracycline (aTC). **c** Michaelis-Menten curves for Tet(X6)-catalyzed degradation of tetracycline antibiotics. Note that the 65 μM data point for eravacycline is omitted for uniform scale on the x-axis and the full plot is provided as Supplementary Fig. 5. **d** Apparent K_m , k_{cat} , and catalytic efficiencies (k_{cat}/K_m) of Tet(X6) against different tetracyclines. Error values represent standard deviations for three independent trials.

Based on the Michaelis-Menten fits for all antibiotic substrates, the range of apparent K_m values was 5–57 within the error of uncertainty ranging from 17–25% for these data fits (Fig. 2d). Among the five substrates studied, tetracycline showed the lowest apparent K_m value of $6 \pm 1 \mu\text{M}$, suggesting the highest apparent binding affinity, followed by tigecycline (apparent $K_m = 12 \pm 3 \mu\text{M}$), omadacycline (apparent $K_m = 18 \pm 3 \mu\text{M}$), and eravacycline (apparent $K_m = 47 \pm 10 \mu\text{M}$). The apparent catalytic efficiency of Tet(X6) was greatest for tetracycline as the substrate ($k_{cat}/K_m = 0.04 \pm 0.01 \text{ min}^{-1} \mu\text{M}^{-1}$) compared to third-generation tetracycline substrates, and is mainly driven by K_m . The apparent catalytic efficiencies (k_{cat}/K_m) for Tet(X6)-catalyzed oxidation of eravacycline ($k_{cat}/K_m = 0.011 \pm 0.004 \text{ min}^{-1} \mu\text{M}^{-1}$), tigecycline ($k_{cat}/K_m = 0.013 \pm 0.004 \text{ min}^{-1} \mu\text{M}^{-1}$), and omadacycline ($k_{cat}/K_m = 0.011 \pm 0.003 \text{ min}^{-1} \mu\text{M}^{-1}$) were similar.

Anhydrotetracycline rescues Tet(X6)-mediated inactivation of tetracycline antibiotics. We have previously established that anhydrotetracycline inhibits a wide range of TDases and therefore can be classified as a pan-TDase inhibitor^{12,19}. Here, we study if anhydrotetracycline can rescue tetracycline activity against *E. coli* producing Tet(X6). We identified anhydrotetracycline concentrations that result in a tetracycline MIC lower than that of tetracycline alone, using checkerboard broth microdilution antibiotic susceptibility assays which test for cell growth in multiple tetracycline-anhydrotetracycline combinations. The addition of 16 μg/mL anhydrotetracycline reduced by 16-fold the concentration of tetracycline required to inhibit growth of Tet(X6)-producing *E. coli*, from 256 μg/mL to 16 μg/mL (Fig. 3a). The calculated fractional inhibitory concentration (FICI) index²⁵ is provided for reference (Fig. 3b).

While anhydrotetracycline has antibiotic activity on its own against *E. coli*, we used concentrations below the MIC (32 μg/mL; Fig. 2b), then evaluated the inhibitory activity of anhydrotetracycline against Tet(X6)-mediated degradation of tetracycline antibiotics (Fig. 3c). The apparent half-maximal inhibitory concentrations (IC₅₀s) observed were in the low micromolar range (2–12 μM), consistent with concentrations used in the

whole cell rescue assays. Together these results suggest that, as with other TDases, anhydrotetracycline inhibition is a promising combination therapy against bacteria producing Tet(X6).

Anhydrotetracycline binds in a substrate-like orientation in type 1 TDases. An X-ray co-crystal structure of anhydrotetracycline in complex with Tet(X6) was determined at 2.2 Å resolution (Table 1). A clear non-protein density was observed in the substrate-binding cavity, consistent with the size and shape of anhydrotetracycline (Fig. 4a). This structure shows that anhydrotetracycline binds in a substrate-like orientation in Tet(X6). The isoalloxazine group of bound FAD occupies an ‘IN’ orientation in the Tet(X6)-anhydrotetracycline complex structure, as observed for the anhydrotetracycline-free structure (Fig. 4a). The anhydrotetracycline binds to Tet(X6) in a substrate-like orientation, placing the A-ring close to the FAD and the D-ring close to the C-terminal bridge helix. The orientation of anhydrotetracycline in Tet(X6) remains conserved in structures of tetracycline substrates in complex with other type 1 TDases, and is likely driven by the shared planarity of rings B, C, and D between anhydrotetracycline and other tetracycline substrates^{14,17,18}.

To compare polar and non-polar interactions of anhydrotetracycline in Tet(X6) with previously studied interactions in other type 1 TDase-substrate complexes, we aligned the Tet(X6)-anhydrotetracycline complex structure to a previously solved X-ray crystal structure of Tet(X) in complex with chlortetracycline (PDB ID: 2Y6R). The protein-ligand interactions between the tetracycline moieties and the residues of type 1 TDases remain conserved in the Tet(X6)-anhydrotetracycline and Tet(X)-chlortetracycline structures¹⁸ (Supplementary Fig. 3). For example, the substitution of the 2,3-enol hydroxyl group at the A-ring of the bound anhydrotetracycline forms a hydrogen bond with side chains of Gln192 (Fig. 4b). The carboxamide carbonyl oxygen at the 2-position of anhydrotetracycline forms a hydrogen bond with Arg213. A water molecule serves as a hydrogen-bonding bridge between the carboxamide substitution of anhydrotetracycline and Thr59. In addition, the Phe224-side chain stabilizes the bound anhydrotetracycline through π -cation interaction with the

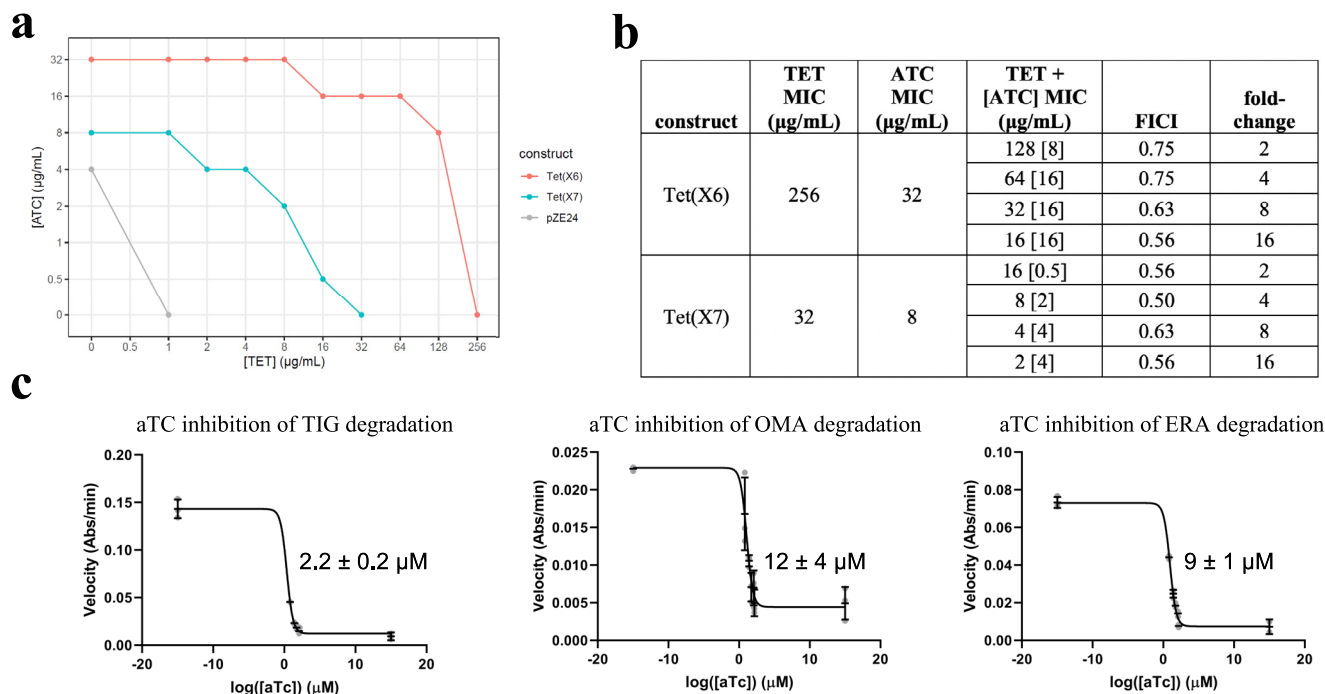


Fig. 3 Anhydrotetracycline rescues Tet(X6)-mediated inactivation of tetracycline antibiotics. **a** Whole cell inhibition of *E. coli* expressing tetracycline destructase enzymes. Abbreviations: tetracycline (TET); anhydrotetracycline (aTC). **b** Calculated FICI. **c** In vitro aTC inhibition of Tet(X6) degradation of tetracycline antibiotics as observed via an optical absorbance assay. IC₅₀ values of each curve are shown. Error values represent standard deviations for three independent trials.

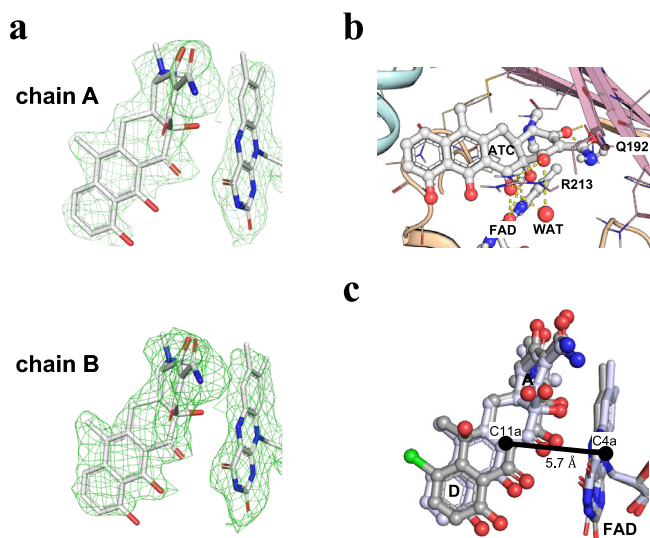


Fig. 4 Anhydrotetracycline binds in a substrate-like orientation in Tet(X6). **a** Polder maps (Fo-Fc map contoured at 3 σ) identify the substrate-like binding orientation of anhydrotetracycline (aTC) in the two chains of the Tet(X6) crystal structure. The complete Polder map is shown in Supplementary Fig. 6. Asymmetric units of anhydrotetracycline-complexed Tet(X6) X-ray crystal structure is shown in Supplementary Fig. 4. **b** Key interactions of anhydrotetracyclines with active site residues of Tet(X6). **c** Aligned crystal structures of Tet(X6)-anhydrotetracycline complex with Tet(X)-chlortetracycline (CTC) complex structure (PDB ID: 2Y6R). Aligned CTC and FAD from Tet(X) structures are shown in grey. The C11a of aTC is at 5.7 Å from C4a of the FAD isoalloxazine ring.

7-dimethylamino substitution of anhydrotetracycline. Further, the isoalloxazine-ring system of FAD forms two additional H-bonds with anhydrotetracycline. The O4 and N5 atoms of FAD form H-bonds to the keto-enol moiety (O12) and nearby hydroxyl group (O12a) of bound anhydrotetracycline. These interactions contribute to orienting the anhydrotetracycline scaffold for hydroxylation by a putative C4a-peroxy-flavin reactive intermediate at site C11a, with at an appropriate short distance of ~ 5.6 Å from the C4a of FAD-isoalloxazine heterocycle. Anhydrotetracycline also makes two H-bonds with aromatic amino acids: hydrogen atom at the C-7 position in the D-ring of anhydrotetracycline with the backbone oxygen atom of Phe319; and oxygen of the carboxamide moiety attached to the C-2 position of the A-ring of anhydrotetracycline with the aromatic hydrogen atom of His234 (Fig. 4b). An alignment of the Tet(X6)-anhydrotetracycline complex with previously solved Tet(X)-chlortetracycline complex (PDB ID: 2Y6R) confirmed a conserved distance of ~ 5.7 Å between C11a of anhydrotetracycline and C4a of the FAD isoalloxazine ring, suggesting a correlation of this binding mode with hydroxylation of C11a across substrate classes (Fig. 4c).

Anhydrotetracycline oxidation is catalyzed by type 1 TDases.

We have previously established that anhydrotetracycline is a pan destructase inhibitor^{10,12} that inhibits diverse type 1 and type 2 TDases. While type 2 TDases cannot metabolize anhydrotetracycline, type 1 TDases such as Tet(X) are capable of slowly turning over anhydrotetracycline as a substrate. The Tet(X6)-anhydrotetracycline complex structure shows a substrate-like binding mode of anhydrotetracycline in Tet(X6). Therefore, we speculated that Tet(X6) can oxidize anhydrotetracycline at the C11a atom (Fig. 5a). To assess the potential for anhydrotetracycline to serve as a substrate for Tet(X6), we performed an in vitro optical absorbance kinetic assay and LC-MS analysis, as previously reported¹². We observed degradation of anhydrotetracycline as indicated by the

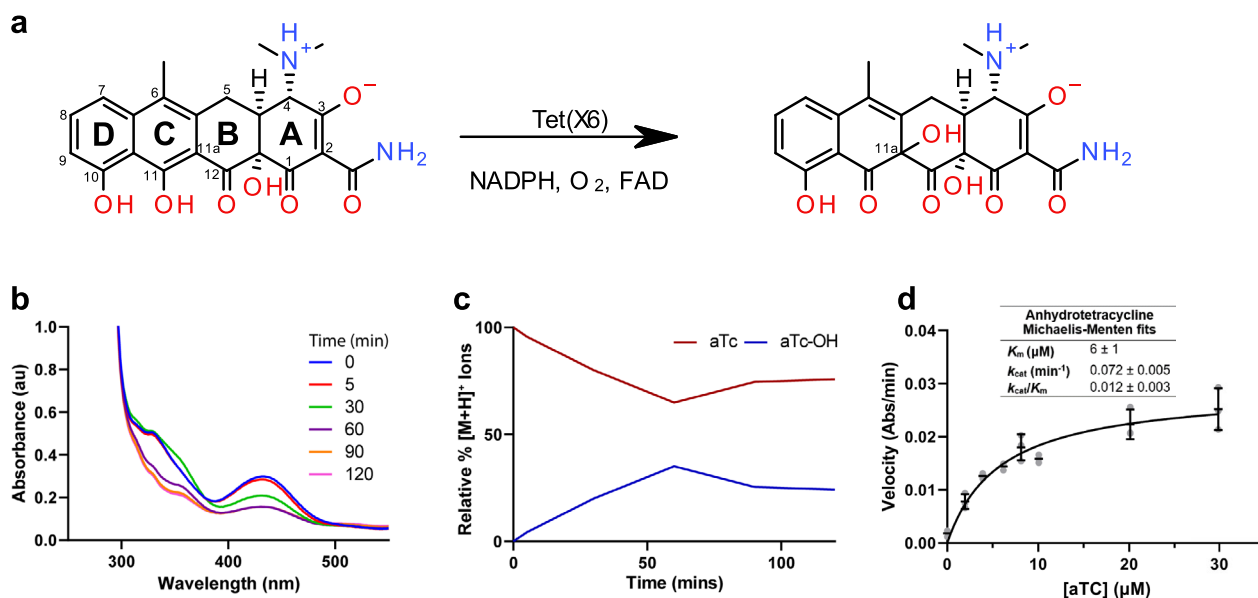


Fig. 5 Anhydrotetracycline oxidation is catalyzed by type 1 TDases. **a** C11a is the plausible site of oxidation in aTC. **b** Degradation of aTC as observed via optical absorbance spectroscopy. **c** Extracted mass ion counts (normalized as relative %) for aTC and oxidized aTC-OH from LC-MS of Tet(X6) reaction from panel (b). **d** Michaelis-Menten steady-state kinetic curve for Tet(X6)-catalyzed degradation of aTC. Error values represent standard deviations for three independent trials.

time-dependent decrease at 440 nm (unique λ_{max} for anhydrotetracycline under assay conditions) in the presence of Tet(X6), NADPH, and O_2 (Fig. 5b). We analyzed the same reaction mixtures by LC-MS and identified ions corresponding to the predicted mass for the $[\text{M} + \text{O} + \text{H}]^+$ molecular ion of oxidized anhydrotetracycline that appeared with stoichiometric loss of the $[\text{M} + \text{H}]^+$ ion corresponding to the parent anhydrotetracycline predicted mass (Fig. 5c). To evaluate the catalytic efficiency of Tet(X6) degradation of anhydrotetracycline, Michaelis-Menten steady-state kinetics were determined (Fig. 5d). The observed apparent binding affinity (K_m) was $6 \pm 1 \mu\text{M}$, similar to tetracycline, but lower than tigecycline (apparent $K_m = 12 \pm 3 \mu\text{M}$), omadacycline (apparent $K_m = 18 \pm 3 \mu\text{M}$), and eravacycline (apparent $K_m = 47 \pm 10 \mu\text{M}$) (Fig. 2d). The apparent k_{cat} for Tet(X6) with anhydrotetracycline as the substrate, however, was significantly lower than tetracycline antibiotic substrates by up to a factor of 7, at $0.072 \pm 0.005 \mu\text{M}$ (Fig. 5d). This implies that the reduced catalytic efficiency of Tet(X6) for turning over anhydrotetracycline ($k_{cat}/K_m = 0.012 \pm 0.003 \text{ min}^{-1} \mu\text{M}^{-1}$) compared to tetracycline ($k_{cat}/K_m = 0.04 \pm 0.01 \text{ min}^{-1} \mu\text{M}^{-1}$) is driven by an apparent reduction in k_{cat} . This is consistent with the model that anhydrotetracycline binds rapidly in the active site of Tet(X6) and serves as a competitive substrate for Tet(X6) with a much lower rate of catalysis (k_{cat}). The binding orientation and enzyme kinetics of anhydrotetracycline in Tet(X6) open new avenues for rational drug design to develop potent anhydrotetracycline-based type 1 TDase inhibitors that further reduce k_{cat} or eliminate catalysis.

Discussion

In this study, we determined X-ray structures of the Type 1 TDase Tet(X6) as a *holo*-enzyme (FAD-bound) and in complex with anhydrotetracycline. The X-ray structure of the Tet(X6)-anhydrotetracycline complex demonstrates a substrate-like binding orientation of anhydrotetracycline, supported by biochemical and cellular studies which indicate a substrate-like metabolism. We established that anhydrotetracycline competitively inhibits Tet(X6)-mediated inactivation of tetracycline antibiotics despite the ability of Tet(X6) to turnover

anhydrotetracycline as a substrate. This type of sacrificial substrate inhibition of enzymes serves as the basis of clinically useful β -lactamase inhibitor/ β -lactam antibiotic combination therapies^{26–31}. The inhibition of β -lactamases is achieved through an initial hydrolysis of the bound inhibitor leading to covalent adduct formation (clavulanic acid and sulbactam) or reversible hydrolysis (avibactam). Here, the inhibition of Tet(X6) by anhydrotetracycline is reversible and the oxidized anhydrotetracycline product is released. Hence, the apparent inhibition of Tet(X6) arises due to the ability of anhydrotetracycline to out-compete tetracycline antibiotics for binding combined with a slower rate of enzymatic turnover of anhydrotetracycline relative to tetracyclines. The sacrificial nature of anhydrotetracycline occupies TDases in bacterial cells to reduce the rate and likelihood of TDase-mediated degradation of tetracycline antibiotics when used in combination therapies. The type 2 TDases cannot metabolize anhydrotetracycline in this manner¹². Type 1 TDases from clinical pathogens contain conserved residues in the FAD-binding pocket and in the substrate-binding pocket, suggesting a shared mechanism of anhydrotetracycline binding and enzyme inhibition^{14,17,18}. Our X-ray crystal structures provide insights into the binding mode of anhydrotetracycline in type 1 TDases and may guide design and development of more potent TDase inhibitors that do not act as sacrificial substrates³².

Multiple recent studies have suggested combination therapy consisting of a tetracycline antibiotic with a TDase inhibitor is also feasible^{12,33–35}. Park et al. reported that anhydrotetracycline can rescue tetracycline efficacy in pathogens expressing Tet(56), a type 2 TDase¹². Markley et al. generated several analogs of anhydrotetracycline with halogenation of the D-ring to extend the spectrum of inhibition against type 1 and type 2 TDases¹⁹. Liu et al. demonstrated that combining antiviral agent azidothymidine (AZT) with tigecycline decreased the survival of *E. coli* expressing Tet(X4)³³. Xu et al. established that plumbagin, a natural naphthoquinone isolated from plants, shows synergistic effects with tetracycline antibiotics against Tet(X3)-/Tet(X4)-producing bacteria³⁴. Deng et al. confirmed a combination of $\text{Bi}(\text{NO}_3)_3$ and tigecycline can prevent development of resistance in bacteria expressing Tet(X)³⁵. Most recently, Williford et al.

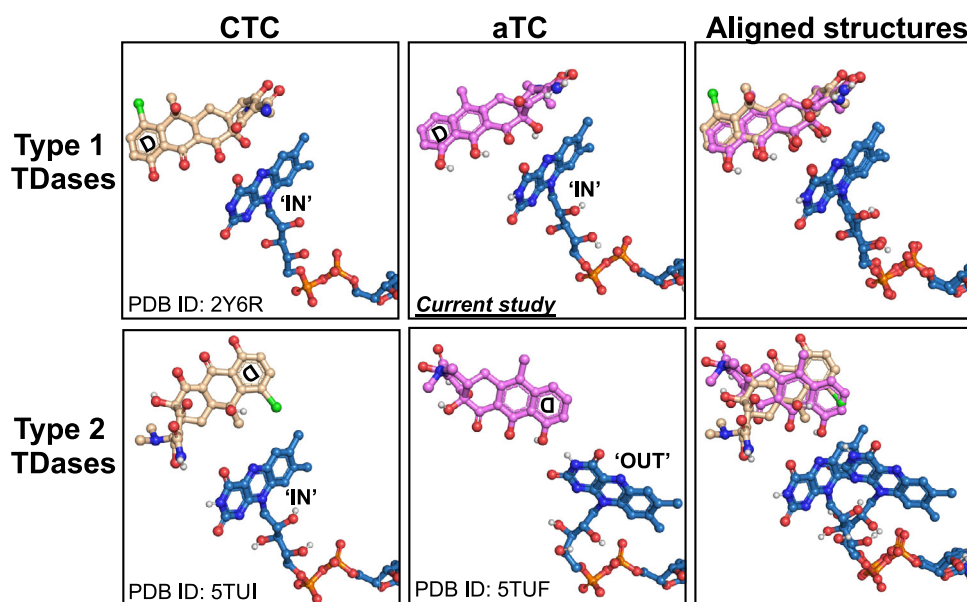


Fig. 6 Substrate and inhibitor binding modes in type 1 and type 2 TDases. In type 1 TDases (top panels), chlortetracycline (CTC) and anhydrotetracycline (aTC) bind in a similar substrate-like orientations. The bound co-factor, FAD (shown in blue) occupies an “IN” orientation. In contrast, CTC and aTC bind in distinct orientations in type 2 TDases (bottom panels). Anhydrotetracycline (aTC) locks FAD in an inactive “OUT” orientation.

reported a series of C9-benzamide and C9-benzylamine anhydrotetracycline analogs that act as bisubstrate inhibitors of type 1 and type 2 TDases³². Despite these recent investigational studies, the structural characteristics of an inhibitor in clinically relevant TDases (i.e., type 1 TDases), remain unknown. Structural insights into TDase-inhibitor complexes are imperative to design potent and effective TDase inhibitors.

The structural architecture of a TDase is composed of three conserved, key features: (i) a Rossman-fold containing FAD-binding domain; (ii) a substrate-binding domain; (iii) and a C-terminal bridge helix (Fig. 1). TDases are broadly classified into two main classes: type 1 TDases (also known as Tet(X)-like¹⁴ TDases) and type 2 TDases (also known as soil-derived¹⁰ TDases). A key structural difference between type 1 and type 2 TDases is an additional C-terminal, ‘gate-keeper’ α -helix present in type 2 TDases¹² (Supplementary Fig. 2). This ‘gate-keeper’ helix regulates substrate loading and catalysis, and may plausibly clash with D-ring substituted tetracyclines that include third-generation tetracyclines. Therefore, type 2 TDases remain inactive against third-generation tetracyclines. In contrast, type 1 TDases that lack the ‘gate-keeper’ C-terminal helix can accommodate D-ring substitutions on the tetracycline moiety and inactivate all available tetracyclines. The dynamics of the bound FAD cofactor also play a critical role in enzyme catalysis/inhibition. During the substrate oxidation step of the catalytic cycle, the FAD occupies an ‘IN’ orientation to position the presumed C4a-peroxy-flavin for oxygen transfer to C11a of the bound substrate. The oxidized FAD transitions to the ‘OUT’ state for subsequent regeneration (presumably reduction by NADPH) and availability for the next round of catalysis.

Prior to this report, no structural details have been available for type 1 TDases in complex with an inhibitor. Anhydrotetracycline is a pan-TDase inhibitor that acts against both classes of TDases in different biochemical and cellular assays^{10,12,14,19}. Here, we have solved the X-ray structure of a type 1 TDase, Tet(X6), in complex with anhydrotetracycline. The Tet(X6)-anhydrotetracycline complex shows the FAD cofactor bound in an ‘IN’ conformation that is distinct from the ‘OUT’ conformation observed for FAD in X-ray structures of type 2 TDases complexed with

anhydrotetracycline. The anhydrotetracycline binds in a substrate-like orientation in the Tet(X6) active site and would compete for binding with diverse tetracycline substrates (Fig. 6)^{17,18}. Steady-state kinetics suggest anhydrotetracycline is a good binding ligand but a poor substrate for catalysis relative to tetracycline antibiotics. The extra site of dehydration at the C5'-C6 bond of anhydrotetracycline creates a more stable aromatic naphthalene moiety compared to the styrene moiety present in tetracyclines. Anhydrotetracycline also benefits from extended conjugation across the sensitive 1,3-diketo/enol system formed by atoms C11-C11a-C12 at the C,D-ring juncture. Oxidation at C11a of anhydrotetracycline and tetracycline presumably occurs via hydroxyl group transfer from the reactive C4a-peroxy-flavin intermediate. The extra stabilization of anhydrotetracycline is likely to reduce the nucleophilicity of the enol tautomer at C11a and slow the rate of oxidation at C11a compared to more reactive tetracycline substrates.

Type 1 TDases are more commonly found in pathogens. Despite conserved residues in the FAD-binding pocket and in substrate-binding pockets, different type 1 TDases show distinct catalytic efficiencies towards different substrates. Mutations in regions distant from ligand binding cavities may plausibly contribute to the difference in structural dynamics and influence local active site structures resulting in different catalytic efficiencies. Indeed, a surface-localized, single point mutation, Thr280Ala in Tet(X2) reduces the apparent K_m for minocycline by two-fold³⁶.

Anhydrotetracycline-based inhibitors have been shown to inhibit diverse TDases in enzymatic and cellular studies^{19,32}. This study provides structural insights into the binding mode of anhydrotetracycline complexed with type 1 TDase Tet(X6), and reveals key pharmacophoric features in the active site cavity, which can be explored further to develop improved anhydrotetracycline-based inhibitors with enhanced binding affinity and enzyme inhibition. Specifically, side chains of Asp61, His63, Asn112, Gln322, Glu367, Asn371 in the vicinity of the D-ring of bound anhydrotetracycline may be targeted to form additional H-bonds with the designed inhibitor through substituents on the D-ring of the anhydrotetracycline scaffold. Similarly, side chains of Asp61 and Arg213 are positioned favorably to form additional H-bonds with polar group

substitutions at the C-ring of the anhydrotetracycline scaffold. Substituents on the B- and A-rings of tetracycline scaffold could possibly form additional H-bonds with the side chains of Ser238, Asn190, His234, Gln192. These findings establish a foundation for rational structure-based design of anhydrotetracycline-based inhibitors to combat antibiotic resistance conferred by type 1 TDases.

Methods

Cloning and protein expression. The coding region of *tet(X6)* (QHN11884.1)²⁰ was cloned in a pET28 vector (cleavage sites: AgeI, KpnI) with a 6-His tag at the C-terminus. The cloned construct was then transformed into *E. coli* BL21 (DE3) to express the protein. Cells were cultured at 37 °C in LB media, containing 0.03 mg/ml kanamycin, until the OD₆₀₀ (optical density at λ = 600 nm) reached 0.6–0.8. At that point, the temperature was lowered to 18 °C and expression was induced with 1 mM Isopropyl β-D-1-thiogalactopyranoside (Sigma-Aldrich, St. Louis, MO). The induced culture was grown overnight (~20 h) at 18 °C and centrifuged at the maximum speed (20 min, 4 °C) to pellet down the cells.

Protein purification. The cell pellet was resuspended in the lysis buffer [50 mM Tris (pH 8.0), 100 mM NaCl, 10 mM imidazole (pH 8.0) 10 mM beta-mercaptoethanol (BME), PierceTM protease inhibitor tablet (catalog # A32963; Thermo Scientific) and stored at –80 °C. To purify the protein, the frozen pellet was thawed in the presence of 0.25 mg/mL lysozyme. The cells were disrupted using a sonicator (ON/OFF/total-time:0.5/0.5/120 s). The cell lysate was centrifuged at 25,000 g for 20 min and the supernatant was loaded on nickel rapid run agarose beads (Goldbio) that were previously equilibrated with the wash buffer [50 mM Tris (pH 8.0), 100 mM NaCl, 10 mM imidazole (pH 8.0), 5 mM BME and PierceTM protease inhibitor tablet (catalog # A32963; Thermo Scientific). The beads were washed three times with five-column volume of wash buffer and finally eluted with 3-column volume of the elution buffer [50 mM Tris (pH 8.0), 100 mM NaCl, 500 mM imidazole (pH 8.0)]. The eluted protein sample was further purified by gel purification using HiLoad 16/600 Superdex 200 pg column (GE Healthcare) equilibrated with 10 mM Hepes (pH 7.4), 100 mM NaCl, 5 mM DTT. The fractions containing the protein of interest were pooled and concentrated using a 10 K MWCO Amicon centrifugal filter (Millipore). During all steps, the sample was kept at 4 °C.

Crystallization, data collection, and structure refinement. Tet(X6) was concentrated to 20 mg/mL and crystallized by vapor diffusion in hanging drop at 18 °C in 0.2 M potassium thiocyanate and 20% (w/v) PEG 3350. Crystals were transferred into 0.2 M potassium thiocyanate, 20% (w/v) PEG 3350 and 20% PEG 400 for 15–30 s and flash-cooled in liquid nitrogen. 4 mM anhydrotetracycline was added to 15 mg/mL Tet(X6), centrifuged at 10,000 g for 10 min at 4 °C, and the complex crystallized by vapor diffusion in hanging drop at 18 °C in 0.2 M potassium thiocyanate and 20% (w/v) PEG 3350. The co-crystals were transferred into 0.2 M potassium thiocyanate, 20% (w/v) PEG 3350 and ethylene glycol for 15–30 s and flash-cooled in liquid nitrogen. Diffraction data were collected at 100 K on beamline 22-ID (APS). 900 frames were collected with the oscillation step of 0.2 degrees. Sample to detector distance was set to 235 mm for anhydrotetracycline-free Tet(X6) crystal and to 250 mm for Tet(X6) + anhydrotetracycline crystal. All data processing and structure analysis were performed using SBGrid³⁷. Diffraction data was reduced and scaled using XDS³⁸. Tet(X6) structure was solved by molecular replacement using Phaser³⁹ with the Tet(X7) structure (PDB ID: 6WG9; sequence identity: ~94%) as a starting model. The protonation pattern of anhydrotetracycline was defined as previously described⁴⁰. Structure refinement was performed in Phenix⁴¹ and Coot⁴². The final model was validated using the Molprobit server⁴³.

Antibiotic susceptibility and checkerboard inhibition assays. Tetracycline resistance genes were cloned into the *KpnI* and *MluI* sites of the pZE24 plasmid (Expressys); this plasmid is maintained using kanamycin and its P_{lac/ara-1} promoter can be regulated with IPTG and arabinose⁴⁴. For high expression, 1 mM IPTG fully relieves repression by LacI⁴⁴ thus only IPTG was used in whole-cell tests. Chemically-competent *E. coli* DH5αZ1 (Expressys) was transformed with these pZE24 constructs by heat shock. Minimum inhibitory concentrations (MICs) were measured as per Clinical and Laboratory Standards Institute (CLSI) guidelines⁴⁵. Substrates and inhibitors were dissolved in DMSO (20 mg/mL) then diluted to working concentrations in cation-adjusted Mueller-Hinton II broth supplemented with 50 µg/mL kanamycin (Supplementary Data 2). Antibiotic susceptibility testing panels were prepared in 96-well flat-bottom microplates (Corning) by two-fold serial dilution of the antibiotic of interest (Supplementary Data 3). For checkerboard whole cell inhibition assays, anhydrotetracycline was two-fold serially diluted in a constant concentration of tetracycline (Supplementary Data 3). Liquid cultures of each strain were grown to exponential phase then diluted to a standard concentration (OD₆₀₀ = 0.0015, which is equivalent to ~5 × 10⁵ CFU/mL) and inoculated into each panel at a 1:1 ratio. Thus, each well had a final concentration of 50 µg/mL kanamycin, 1 mM IPTG, ~5 × 10⁵ CFU/mL (0.5 MacFarland) cells, and variable concentrations of the antibiotic of interest or anhydrotetracycline

(Supplementary Data 2 and 3). Each strain-antibiotic/inhibitor combination was tested in triplicate, along with no-drug and no-cell controls. Inoculated panels were sealed with Breathe-Easy membranes (Sigma-Aldrich) and incubated at 37 °C for 20 h. MICs were scored by absorbance measurements at 600 nm (OD₆₀₀) using the Synergy H1 microplate reader (Biotek Instruments, Inc). Synergy of inhibitor and tetracycline combinations was determined using the fractional inhibitory concentration index (FICI) method²⁵ where FICI > 1 indicates antagonism, FICI = 1 indicates additivity, and FICI < 1 indicates synergy:

$$FICI = \frac{MIC A_{combo}}{MIC A_{alone}} + \frac{MIC B_{combo}}{MIC B_{alone}} \quad (1)$$

Characterization of substrate degradation by scanning optical absorbance spectroscopy and LC-MS. All in vitro kinetic assays were prepared open to air in non-degassed buffer solutions at room temperature. TDase reactions were prepared in 100 mM TAPS buffer (pH 8.5) with an NADPH regenerating system (40 mM glucose-6-phosphate, 4 mM NADP⁺, 1 mM MgCl₂, 4 U/mL glucose-6-phosphate dehydrogenase), 20 µM substrate and 0.24 µM Tet(X6) (all concentrations represent final working concentrations). In vitro reactions were monitored by optical absorbance spectroscopy on an Agilent Cary 50 UV-visible spectrophotometer using polystyrene cuvettes. Reaction progress was monitored by optical absorbance spectroscopy (280–550 nm, 1 nm and 5 min intervals) over 2 h. Aliquots of reaction sample (150 µL) were removed and quenched (600 µL of 1:1 acetonitrile/0.25 M aqueous HCl) immediately after enzyme was added (0 min) and at 5, 30, 60, 90, and 120 min intervals. The quenched samples were centrifuged (5000 rpm, 4 °C) for 5 min, and 600 µL of the resulting supernatant was mixed with an Fmoc-Ala internal standard (3.12 µM final concentration) and analyzed by LC-MS in positive ion mode (single trial). LC-MS was acquired using an Agilent 6130 single quadrupole instrument (ESI +) with G1313 autosampler, G1315 diode array detector, and 1200 series solvent module with separation on a Phenomenex Gemini C18 column, 50 × 2 mm (5 µm) fit with a guard column cassette. LCMS solvents were 0.1% formic acid in H₂O (A) and 0.1% formic acid in acetonitrile (B). Solvent gradient was linear starting from 0% B to 95% B over 20 min at a flow rate of 0.5 mL/min. LCMS data were processed using ChemStation software version B.04.02 SP1. Extracted ion chromatograms (EICs) for the expected [M + H]⁺ molecular ions corresponding to substrate and mono-hydroxylated product were normalized to the [M + H]⁺ counts for an Fmoc-Ala internal standard.

Characterization of steady-state kinetics for substrate inactivation. All experiments were prepared open to air in non-degassed buffer solutions at room temperature. Reactions were prepared in 100 mM TAPS buffer at pH 8.5 with 0–30 µM substrate (a 65 µM concentration was included for eravacycline to reach v_{max}), 504 µM NADPH, 5.04 mM MgCl₂, and 0.4 µM Tet(X6) (final working concentrations). Reactions were initiated by the addition of Tet(X6) and were monitored continuously via optical absorbance spectroscopy at 400 nm (440 nm for aTC inactivation) for 2 min (performed in triplicate as independent trials). Initial enzyme velocities were determined by linear regression using Agilent Cary WinUV Software over the linear range of the reaction (typically between 0 to 1 min), plotted against the concentration of the substrate, and fitted to the Michaelis–Menten or allosteric sigmoidal nonlinear regression equations using GraphPad Prism 6.

Determination of apparent Tet(X6) inhibitor IC₅₀ values. All experiments were prepared open to air in non-degassed buffer solutions at room temperature. Half-maximal inhibitory concentrations (IC₅₀) for the inhibition of Tet(X6) were determined from the velocities of substrate degradation in the presence of varying concentrations of inhibitor. Reaction samples were prepared in 100 mM TAPS buffer (pH 8.5) with 504 µM NADPH, 5.04 mM MgCl₂, 25.3 µM TC, varying concentrations of inhibitor (typically 0–146 µM), and 0.4 µM Tet(X6) (final working concentrations). Reactions were initiated by the addition of Tet(X6) and were monitored continuously via optical absorbance spectroscopy at 400 nm for 2 min (performed in triplicate as independent trials). Initial enzyme velocities were determined by linear regression using Agilent Cary WinUV Software over the linear range of the reaction (typically between 0 to 1 min). The velocities were plotted against the logarithm of inhibitor concentration, and apparent IC₅₀ values were determined using nonlinear regression analysis in GraphPad Prism v6. Each set of experiments included a no-TDase control reaction which was used as the full enzyme inhibition velocity and assigned to an inhibitor concentration of 1 × 10¹⁵, as well as a no-inhibitor control which was assigned an inhibitor concentration of 1 × 10⁻¹⁵. A no-TC control was also performed to search for potentially competitive background signals generated from the enzymatic degradation of the inhibitor itself. For all inhibitor-enzyme combinations, the initial velocities of the no-TC controls were negligible.

Statistics and reproducibility. X-ray structural analysis statistics including number of crystals used per data set are include in Table 1. Standard statistical analysis for X-ray diffraction data processing and analysis were adhered to and presented in Table 1. Enzyme assays were performed in two or three independent trials and whole cell inhibition assays were performed in triplicate.

Reporting summary. Further information on research design is available in the Nature Portfolio Reporting Summary linked to this article.

Data availability

Atomic coordinates and structure factors have been deposited in the Protein Data Bank with the accession codes 8ER1 and 8ER0. All other data generated or analyzed during this study are included in this published article and its supplementary information files. Source data for figures can be found in Supplementary Data 4.

Received: 22 July 2022; Accepted: 31 March 2023;

Published online: 17 April 2023

References

1. Tatsuta, K. Total synthesis of the big four antibiotics and related antibiotics. *J. Antibiot. (Tokyo)* **66**, 107–129 (2013).
2. Chopra, I. & Roberts, M. Tetracycline antibiotics: mode of action, applications, molecular biology, and epidemiology of bacterial resistance. *Microbiol. Mol. Biol. Rev.* **65**, 232–260 (2001).
3. Sum, P. E. & Petersen, P. Synthesis and structure-activity relationship of novel glycylicycline derivatives leading to the discovery of GAR-936. *Bioorg. Med. Chem. Lett.* **9**, 1459–1462 (1999).
4. Draper, M. P. et al. Mechanism of action of the novel aminomethylcycline antibiotic omadacycline. *Antimicrob. Agents Chemother.* **58**, 1279–1283 (2014).
5. Thakare, R., Dasgupta, A. & Chopra, S. Eravacycline for the treatment of patients with bacterial infections. *Drugs Today (Barc.)* **54**, 245–254 (2018).
6. Kelesidis, T., Karageorgopoulos, D. E., Kelesidis, I. & Falagas, M. E. Tigecycline for the treatment of multidrug-resistant Enterobacteriaceae: a systematic review of the evidence from microbiological and clinical studies. *J. Antimicrob. Chemother.* **62**, 895–904 (2008).
7. Karageorgopoulos, D. E. & Falagas, M. E. Current control and treatment of multidrug-resistant *Acinetobacter baumannii* infections. *Lancet Infect. Dis.* **8**, 751–762 (2008).
8. Speer, B. S. & Salyers, A. A. Characterization of a novel tetracycline resistance that functions only in aerobically grown *Escherichia coli*. *J. Bacteriol.* **170**, 1423–1429 (1988).
9. Speer, B. S. & Salyers, A. A. Novel aerobic tetracycline resistance gene that chemically modifies tetracycline. *J. Bacteriol.* **171**, 148–153 (1989).
10. Forsberg, K. J., Patel, S., Wenczewicz, T. A. & Dantas, G. The tetracycline destructases: a novel family of tetracycline-inactivating enzymes. *Chem. Biol.* **22**, 888–897 (2015).
11. Yang, W. et al. TetX is a flavin-dependent monooxygenase conferring resistance to tetracycline antibiotics. *J. Biol. Chem.* **279**, 52346–52352 (2004).
12. Park, J. et al. Plasticity, dynamics, and inhibition of emerging tetracycline resistance enzymes. *Nat. Chem. Biol.* **13**, 730–736 (2017).
13. He, T. et al. Emergence of plasmid-mediated high-level tigecycline resistance genes in animals and humans. *Nat. Microbiol.* **4**, 1450–1456 (2019).
14. Gasparrini, A. J. et al. Tetracycline-inactivating enzymes from environmental, human commensal, and pathogenic bacteria cause broad-spectrum tetracycline resistance. *Commun. Biol.* **3**, 241 (2020).
15. Sun, J. et al. Plasmid-encoded tet(X) genes that confer high-level tigecycline resistance in *Escherichia coli*. *Nat. Microbiol.* **4**, 1457–1464 (2019).
16. Forsberg, K. J. et al. The shared antibiotic resistance of soil bacteria and human pathogens. *Science* **337**, 1107–1111 (2012).
17. Cheng, Q. et al. Structural and mechanistic basis of the high catalytic activity of monooxygenase Tet(X4) on tigecycline. *BMC Biol.* **19**, 262 (2021).
18. Volkers, G., Palm, G. J., Weiss, M. S., Wright, G. D. & Hinrichs, W. Structural basis for a new tetracycline resistance mechanism relying on the TetX monooxygenase. *FEBS Lett.* **585**, 1061–1066 (2011).
19. Markley, J. L. et al. Semisynthetic analogues of anhydrotetracycline as inhibitors of tetracycline destructase enzymes. *ACS Infect. Dis.* **5**, 618–633 (2019).
20. He, D. et al. A novel tigecycline resistance gene, tet(X6), on an SXT/R391 integrative and conjugal element in a *Proteus* genomospes 6 isolate of retail meat origin. *J. Antimicrob. Chemother.* **75**, 1159–1164 (2020).
21. Linkevicius, M., Sandegren, L. & Andersson, D. I. Potential of tetracycline resistance proteins to evolve tigecycline resistance. *Antimicrob. Agents Chemother.* **60**, 789–796 (2016).
22. Volkers, G. et al. Putative dioxygen-binding sites and recognition of tigecycline and minocycline in the tetracycline-degrading monooxygenase TetX. *Acta Crystallogr. D. Biol. Crystallogr.* **69**, 1758–1767 (2013).
23. CLSI. Methods for dilution antimicrobial susceptibility tests for bacteria that grow aerobically, M07Ed11. *Wayne, PA: Clinical and Laboratory Standards Institute* (2018).
24. Omadacycline (Nuzyla) - A New Tetracycline Antibiotic. *JAMA* **322**, 457–458 <https://doi.org/10.1001/jama.2019.8199> (2019).

25. Berenbaum, M. C. A method for testing for synergy with any number of agents. *J. Infect. Dis.* **137**, 122–130 (1978).
26. Wright, G. D. Antibiotic adjuvants: rescuing antibiotics from resistance: (Trends in Microbiology 24, 862–871 October 17, 2016). *Trends Microbiol.* **24**, 928 (2016).
27. Chakradhar, S. What's old is new: reconfiguring known antibiotics to fight drug resistance. *Nat. Med.* **22**, 1197–1199 (2016).
28. Gill, E. E., Franco, O. L. & Hancock, R. E. Antibiotic adjuvants: diverse strategies for controlling drug-resistant pathogens. *Chem. Biol. Drug Des.* **85**, 56–78 (2015).
29. Bernal, P., Molina-Santiago, C., Daddaoua, A. & Llamas, M. A. Antibiotic adjuvants: identification and clinical use. *Micro. Biotechnol.* **6**, 445–449 (2013).
30. Reading, C. & Cole, M. Clavulanic acid: a beta-lactamase-inhibiting beta-lactam from *Streptomyces clavuligerus*. *Antimicrob. Agents Chemother.* **11**, 852–857 (1977).
31. Zhanel, G. G. et al. Ceftazidime-avibactam: a novel cephalosporin/β-lactamase inhibitor combination. *Drugs* **73**, 159–177 (2013).
32. Wiliford, E. E. et al. Structure-based design of bisubstrate tetracycline destructase inhibitors that block flavin redox cycling. *J. Med. Chem.* **66**, 3917–3933 (2023).
33. Liu, Y. et al. Anti-HIV agent azidothymidine decreases Tet(X)-mediated bacterial resistance to tigecycline in *Escherichia coli*. *Commun. Biol.* **3**, 162 (2020).
34. Xu, L. et al. A novel inhibitor of monooxygenase reversed the activity of tetracyclines against tet(X3)/tet(X4)-positive bacteria. *EBioMedicine* **78**, 103943 (2022).
35. Deng, T. et al. Bismuth drugs reverse tet(X)-conferred tigecycline resistance in gram-negative bacteria. *Microbiol. Spectr.* **10**, e0157821 (2022).
36. Walkiewicz, K. et al. Small changes in enzyme function can lead to surprisingly large fitness effects during adaptive evolution of antibiotic resistance. *Proc. Natl Acad. Sci. USA* **109**, 21408–21413 (2012).
37. Morin, A. et al. Collaboration gets the most out of software. *Elife* **2**, e01456 (2013).
38. Kabsch, W. Xds. *Acta Crystallogr. D. Biol. Crystallogr.* **66**, 125–132 (2010).
39. McCoy, A. J. et al. Phaser crystallographic software. *J. Appl. Crystallogr.* **40**, 658–674 (2007).
40. Aleksandrov, A., Proft, J., Hinrichs, W. & Simonson, T. Protonation patterns in tetracycline: tet repressor recognition: simulations and experiments. *Chembiochem* **8**, 675–685 (2007).
41. Adams, P. D. et al. PHENIX: a comprehensive Python-based system for macromolecular structure solution. *Acta Crystallogr. D. Biol. Crystallogr.* **66**, 213–221 (2010).
42. Emsley, P. & Cowtan, K. Coot: model-building tools for molecular graphics. *Acta Crystallogr. D. Biol. Crystallogr.* **60**, 2126–2132 (2004).
43. Chen, V. B. et al. MolProbity: all-atom structure validation for macromolecular crystallography. *Acta Crystallogr. D. Biol. Crystallogr.* **66**, 12–21 (2010).
44. Lutz, R. & Bujard, H. Independent and tight regulation of transcriptional units in *Escherichia coli* via the LacR/O, the TetR/O and AraC/I1–I2 regulatory elements. *Nucleic Acids Res.* **25**, 1203–1210 (1997).
45. CLSI. Performance Standards for Antimicrobial Susceptibility Testing. *Wayne, PA: Clinical and Laboratory Standards Institute* (2019).

Acknowledgements

We thank the staff members of the SER-CAT beamline at the Advanced Photon Source, Argonne National Laboratory for beamline support. Data were collected at Southeast Regional Collaborative Access Team (SER-CAT) beamlines 22-ID and 22-BM at the Advanced Photon Source, Argonne National Laboratory. SER-CAT is supported by its member institutions (see www.ser-cat.org/members.html), and equipment grants (S10_RR25528, S10_RR028976 and S10_OD027000) from the National Institutes of Health. This study used the Office of Cyber Infrastructure and Computational Biology (OCICB) High Performance Computing (HPC) cluster at the National Institute of Allergy and Infectious Diseases (NIAID), Bethesda, MD. We thank J. Patrick Gorres of (LMIV, NIAID) for copyediting the manuscript. This work was supported by the Intramural Research Program and the Extramural Research Program of the National Institute of Allergy and Infectious Diseases of the National Institutes of Health. N.H.T. is supported by the Intramural Research Program of, National Institutes of Health. G.D. and T.A.W. are supported by an award from the National Institute of Allergy and Infectious Diseases (2U01AI123394). K.S.B. is supported by the National Institute of Diabetes and Digestive and Kidney Diseases (T32-DK007130; PI: N. Davidson). E.E.W. is supported by the National Science Foundation through an NSF-GRFP fellowship (DGE-2139839). The content is solely the responsibility of the authors and does not necessarily represent the official views of the funding agencies.

Author contributions

H.K., G.D., T.A.W., and N.H.T. conceived and designed the study. H.K. expressed, purified and crystallized Tet(X6). H.K. harvested the cryo-protected crystals and collected X-ray data. H.K. solved and refined the structures, and deposited them under the supervision of N.H.T. K.S.B. generated the *E. coli* strains and performed the antibiotic susceptibility and checkerboard inhibition assays. E.E.W. performed enzyme kinetic assays and LC-MS analyses. B.V.-D. assisted with enzyme kinetic assays. G.D., T.A.W.

and N.H.T. supervised the studies. H.K. and N.H.T. wrote the manuscript with input and approval from all authors.

Competing interests

N.H.T., G.D., and T.A.W. declare the following competing interests: N.H.T., G.D., and T.A.W. are listed as co-inventors on US patent number US-10273468-B2. All other authors declare no competing interests.

Additional information

Supplementary information The online version contains supplementary material available at <https://doi.org/10.1038/s42003-023-04792-4>.

Correspondence and requests for materials should be addressed to Gautam Dantas, Timothy A. Wencewicz or Niraj H. Tolia.

Peer review information *Communications Biology* thanks the anonymous reviewers for their contribution to the peer review of this work. Primary Handling Editors: Wendy Mok and Gene Chong.

Reprints and permission information is available at <http://www.nature.com/reprints>

Publisher's note Springer Nature remains neutral with regard to jurisdictional claims in published maps and institutional affiliations.



Open Access This article is licensed under a Creative Commons Attribution 4.0 International License, which permits use, sharing, adaptation, distribution and reproduction in any medium or format, as long as you give appropriate credit to the original author(s) and the source, provide a link to the Creative Commons license, and indicate if changes were made. The images or other third party material in this article are included in the article's Creative Commons license, unless indicated otherwise in a credit line to the material. If material is not included in the article's Creative Commons license and your intended use is not permitted by statutory regulation or exceeds the permitted use, you will need to obtain permission directly from the copyright holder. To view a copy of this license, visit <http://creativecommons.org/licenses/by/4.0/>.

This is a U.S. Government work and not under copyright protection in the US; foreign copyright protection may apply 2023, corrected publication 2023